INVITED PAPER

Isoteric heat of hydrogen adsorption on MOFs: comparison between adsorption calorimetry, sorption isosteric method, and analytical models

A. F. Kloutse[1] · R. Zacharia[1] · D. Cossement[1] · R. Chahine[1] · R. Balderas-Xicohténcatl[2] ·
H. Oh[2] · B. Streppel[2] · M. Schlichtenmayer[2] · M. Hirscher[2]

Abstract Isosteric heat of adsorption is an important parameter required to describe the thermal performance of adsorptive storage systems. It is most frequently calculated from adsorption isotherms measured over wide ranges of pressure and temperature, using the so-called adsorption isosteric method. Direct quantitative estimation of isosteric heats on the other hand is possible using the coupled calorimetric–volumetric method, which involves simultaneous measurement of heat and adsorption. In this work, we compare the isosteric heats of hydrogen adsorption on microporous materials measured by both methods. Furthermore, the experimental data are compared with the isosteric heats obtained using the modified Dubinin–Astakhov, Tóth, and Unilan adsorption analytical models to establish the reliability and limitations of simpler methods and assumptions. To this end, we measure the hydrogen isosteric heats on five prototypical metal–organic frameworks: MOF-5, Cu-BTC, Fe-BTC, MIL-53, and MOF-177 using both experimental methods. For all MOFs, we find a very good agreement between the isosteric heats measured using the calorimetric and isosteric methods throughout the range of loading studied. Models' prediction on the other hand deviates from both experiments depending on the MOF studied and the range of loading. Under low-loadings

of less than 5 mol kg^{-1}, the isosteric heat of hydrogen adsorption decreases in the order Cu-BTC > MIL-53 > MOF-5 > Fe-BTC > MOF-177. The order of isosteric heats is coherent with the strength of hydrogen interaction revealed from previous thermal desorption spectroscopy measurements.

1 Introduction

Cryo-sorption of hydrogen in adsorbent-filled type I light-weight hydrogen tanks is an evolving state-of-the-art technology for vehicular energy storage applications [1]. An important aspect of the adsorptive storage is that adsorption generates heat inside the tank which, if not dissipated effectively, will deteriorate the storage system's overall performance and efficiency [2]. Development and optimization of thermal management designs for cryo-sorptive storage tanks require computational models that predict spatial distribution and temporal evolution of the internal temperatures and total heats of the tank during different hydrogen-filling and drive cycle scenarios [3, 4]. Central to developing such models is the availability of a primitive set of adsorbent's physicochemical and thermophysical properties, such as isosteric heat of adsorption q_{st} and specific heat capacity C_p, evident from the standard energy conservation equation [5] (Eq. 1) typically used to describe the evolution of the sorbent bed temperature [3, 4]:

$$\left(\rho C_p\right)_{eq}\frac{\partial T}{\partial t} + \rho C_p \vec{u} \cdot \nabla T = \nabla \cdot \left(k_{eq} \nabla T\right) + \rho_p \varepsilon_p \frac{\partial n_a}{\partial t} q_{st}.$$

(1)

Isosteric heat of adsorption, the molar enthalpy change when an adsorbate is brought from the gas the phase to

✉ R. Zacharia
renju.zacharia@uqtr.ca

1 Institut de recherche sur l'hydrogène, Université du Québec à Trois-Rivières, Trois-Rivières, QC G9A 5H7, Canada

2 Max-Planck Institute for Intelligent Systems, Heisenbergstrasse 3, 70569 Stuttgart, Germany

form the adsorbed phase, is an important heat term necessary to describe the thermal performance of a storage system; other terms are the conductive, convective, and compression heats. In fact, for hydrogen storage systems based on metal–organic frameworks (MOFs), q_{st} is the most significant heat-generating term in the adsorbent bed [3, 4]. For stationary charging of hydrogen into a MOF-5 tank maintained at 80 K, isosteric heat alone can raise the temperature by ~ 40 % [4] which reduces the net deliverable capacity. While this reinforces the necessity of good thermal management in adsorptive hydrogen storage tanks, it also points out the importance of reliable estimates of adsorption isosteric heats. In Refs. [3, 4] isosteric heats of MOF-5 used were adsorption-dependent ones calculated using an explicit analytical function derived by applying the Clausius–Clapeyron relation to the modified Dubinin–Astakhov (D–A) model [4]. The required model parameters were initially obtained through nonlinear regression of experimental excess hydrogen adsorption data. As the modified D–A model does not reduce to Henry's law at the limit of zero coverage, the isosteric heat behaves as an ill-defined function in the vicinity of $n_a = 0$, which is characterized by a logarithmic singularity [4, 6]. Furthermore, the isosteric heats calculated using adsorption models, including the modified D–A model, are somewhat arbitrary as they depend on adsorption volume which is purely parametric and whose interpretation continues to be debated [7]. In another work, Xiao et al. [8] used coverage-independent isosteric heat of adsorption to develop a parametric model of activated carbon-based hydrogen storage system. While the authors assumed the isosteric heat to be independent of the loading, in reality the heat decreases for energetically heterogeneous adsorbent, such as activated carbon due to the preferential filling of most energetically favorable sites at the onset of adsorption. For a prototypical adsorbent material MOF-5, the reported isosteric heat varies between 3.8 and 5.2 kJ mol^{-1} [9–15].

In the context of isosteric heat of gas–solid adsorption equilibrium, the adsorption implies the absolute amount, n_a which is the quantity of adsorptive species transferred from the gas phase into the adsorbed phase. Since n_a cannot be directly measured using experiments, it is obtained alternatively either by nonlinear regression of experimental excess adsorption using different thermodynamic adsorption models or by assuming liquid density for adsorbed hydrogen. In the past, several models, including the modified D–A [6, 7, 10], multi-potential theory of adsorption (MPTA) [7], Unilan [7, 10] and, Tóth model [10], have been employed to estimate the absolute adsorption. Another approach to estimate the absolute adsorption, as mentioned above, is to assume that the adsorbed hydrogen manifests as a quasi-liquid state with a pressure invariant density ($\rho_l = 0.07$ g ml^{-1}) [16–18]. Under this simple assumption, $n_a = n_{ex} \times (1 - \rho_g/\rho_l)^{-1}$, where ρ_l is the gas-phase hydrogen density. Meanwhile, a survey of the majority of published MOFs' isosteric heats reported in a comprehensive review [9] indicates that more than 90 % (out of ~ 40 reported measurements) of data are estimated directly from excess adsorption isotherms avoiding absolute adsorption altogether, which some literature calls "isoexcess heat" [19].

The two most established experimental techniques available for measuring the isosteric heats are the direct measurement using the coupled calorimetric–volumetric system and the indirect determination from the adsorption isotherms collected at widely different temperatures. In the former approach, also known as adsorption calorimetry, the heat released during adsorption is quantitatively measured using a calorimeter, while the adsorption is simultaneously measured volumetrically. In the second method, which is also known as sorption isosteric method, the heat of adsorption is calculated using Clausius–Clapeyron thermodynamic relation applied to adsorption isotherms collected over wide ranges of pressure and temperature. In its simplest form, this involves graphically determining the slope of $\ln(p)$ versus $1/T$ evaluated at constant n_a using the Clausius–Clapeyron relation [20]. Since experimental adsorption isotherms collected at different temperatures are not necessarily measured at constantly spaced n_a intervals, it is necessary to fit the isotherms that interpolate the isotherm data points, which is very sensitive to errors in equilibrium pressure [20]. Results of measurements by calorimetric and isosteric methods often deviate by as much as 100 % [21]. Although the direct calorimetric measurement is considered to be more accurate than sorption isosteric methods as it does not require approximations related to the linearity of isosteres, the latter approach is "the most popular" method, reasons being the simplicity of the approach and the ubiquitous availability of volumetric/gravimetric experimental setups. Up to 87 % of the isosteric heats reported in Ref. [9] are determined using isosteric method, while only 4 % is determined calorimetrically. In addition to these experimental methods, there also exist certain thermodynamic adsorption models which can be used to derive explicit analytical expression of isosteric heats, either by applying the respective models' empirical expression of absolute adsorption to Clausius–Clapeyron thermodynamic relation or by applying adsorption potential in the isotherm model. This approach is widely used among system developers due to the ease of implementing them in application-level modelling of overall hydrogen storage systems.

In Fig. 1, various schemes generally used to determine adsorption heats from both techniques are given.

The aim of this work is to compare the isosteric heats of hydrogen adsorption on microporous materials measured
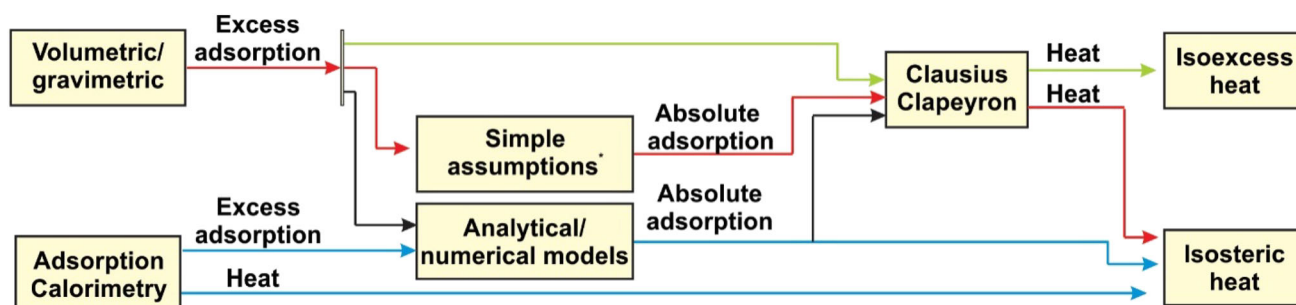
Fig. 1 Various experimental schemes of determining adsorption heats: On one end, volumetric/gravimetric measurement of excess adsorption isotherms coupled with simple assumptions is used in conjunction with Clausius–Clapeyron equation (highlighted in *red*), while on the other end, calorimetric measurements where the excess and heat are directly measured (*blue arrows*). Corresponding absolute adsorption is obtained using analytical or numerical thermodynamic models. *Simple assumptions, such as ideal gas behavior for gas phase and liquid density for adsorbed hydrogen, are typically used in volumetric/gravimetric methods. More than 90 % of isosteric heat measurements reported in Ref. [9], nevertheless, uses excess adsorption with Clausius–Clapeyron equation to generate what is known as the isoexcess heat (*green*)

directly using calorimetry (blue lines in Fig. 1) with those obtained using indirect sorption isosteric method (red line in Fig. 1) and using analytical models so that the reliability and limitations of simpler methods and assumptions can be understood. To this end, we measure the hydrogen isosteric heats on five prototypical metal–organic frameworks: MOF-5, Cu-BTC, Fe-BTC, MIL-53, and MOF-177 using both experimental methods. For the first approach, the absolute adsorption is derived using the analytical Tóth adsorption model, while for the second method, the same is derived by assuming a constant liquid density for adsorbed hydrogen. In addition, the gas density used in the former approach is the real gas density of hydrogen calculated from the real gas EOS implemented in the NIST REFPROP Standard reference database [22], while for the latter, the gas density corresponding to ideal gas and a compressibility factor correction is used. The experimental data are further compared with the isosteric heats obtained using explicit analytical expression of modified D–A, Tóth, and Unilan adsorption model which are derived from both the Clausius–Clapeyron thermodynamic relation and Tóth's potential function (TPF) [23].

2 Experimental

2.1 Measurement of adsorption isotherms and isosteric heats

2.1.1 Direct isosteric heat measurement: adsorption calorimetry

Cu-BTC, Fe-BTC, and MIL-53 were purchased from Sigma-Aldrich. MOF-5 and MOF-177 were synthesized and activated following procedures reported elsewhere [24–26]. Direct calorimetric measurements were performed

using a calibrated adiabatic calorimeter. Schematic details of the system, calibration, and sample transfer details are provided in the supplementary information. After outgassing, samples were cooled down to the working temperature, typically around 77 K, using a liquid nitrogen cooling system. We followed point-by-point introduction of sorbent gas (99.999 % hydrogen) into the dosing manifold [27]. Once the pressure is stabilized in this volume, a needle valve between the sample cell and dosing reservoir was opened to expose an otherwise thermally equilibrated sample (baseline). This is done slowly to ensure reversible expansion. Each introduction of dosing gas led to an instantaneous exothermic heat flow and subsequent relaxation to the baseline. The subsequent doses were introduced once thermodynamic equilibrium was attained. Additional calorimetric measurements were carried out at temperatures 87, 97, 100, 113, 117, and 298 K.

2.1.2 Indirect isosteric heat measurement: isosteric method

Commercially available samples of Cu-BTC, MOF-5, MOF-177, and MIL-53 were provided by BASF SE, while the sample Fe-BTC-xerogel was kindly provided by S. Kaskel, Technical University of Dresden. In all cases, the sample mass was between 100 and 400 mg, and the samples were activated in high vacuum at temperature range of 150–200 °C for several hours, and specific details of the synthesis and activation conditions are reported elsewhere [13, 16].

Isotherm adsorption experiments were performed using an automated Sieverts' apparatus (Setaram-HyEnergy PCTPro-2000) equipped with a so-called microdoser (MD) from HyEnergy for measurements of small amounts of material with a maximum pressure of 20 bar. Independent measurements of isotherms were carried out at 77, 87, 97,

107, 117, and 296 K. In all cases the samples were evacuated at room temperature overnight between each experiment. The adsorbed amount of hydrogen is determined by the volumetric technique based on the gas expansion from a known reservoir volume to the sample holder. The non-adsorbed amount of hydrogen in the sample holder volume is then subtracted based on a calibration performed for each temperature, and the skeletal volume of the sample was measured by a helium expansion test. Additional details of the experimental device and the calibration procedure are provided in the supplementary information.

3 Results and discussion

3.1 Adsorption calorimetry

As the hydrogen gas is introduced into the sample cell, an exothermic heat flow occurs which subsequently undergoes relaxation to the baseline shown in Fig. 2.

For the cell containing MOFs, the exothermic heat flow has two contributions: isosteric heat of adsorption and pressure volume work due to compression of nonideal hydrogen gas [4]. Numerical integration of each heat flow (HF) profile between the time of departure from and return to baseline provides the total heat associated with incremental amount adsorbed during each step [27–29]. This integral corresponds to the area under the profiles in Fig. 2. To calculate the isosteric heat contribution, it is necessary to account for also the heats due to in-flow of warm hydrogen and compression work, which is typically known as the "spurious heat" [30]. This is done by performing expansion experiments with a blank cell. Since the volume available for the gas expansion is different when experiments are performed with and without adsorbent, an appropriate correction must be made. The broken lines in Fig. 2 correspond to the heat flow data in the blank cell where the heat flow arises due only to the heat contribution from warm hydrogen flow and compression heat. The decay of the heat flow rate (HF) follows an exponential-type function (see Supplementary Information)

The net heat due to isosteric heat decreases for successive adsorption steps and reaches a plateau (inset of Fig. 2). This is attributed to lesser amount of adsorption (n_a) with each expansion steps; in contrast, the spurious heat contribution increases initially and remains almost constant with the dosing steps. With each adsorption steps, the relative significance of the pressure work increases as the ratio of gas stored in adsorbed phase to that stored in the gas phase decreases, which is coherent with the analysis of Hardy et al. [3].

For small step changes of pressure, the heat dissipated due to pressure volume work during a reversible expansion
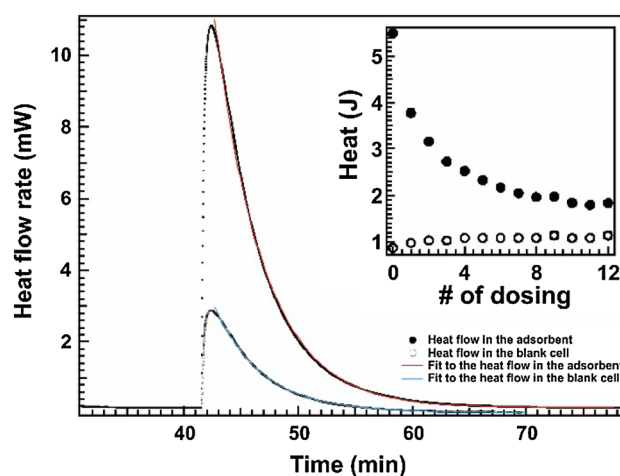

Fig. 2 Characteristic exothermic heat flow and relaxation signals when hydrogen gas is introduced into the calorimetric cell containing Cu-BTC (*filled circles*) and blank cell (*open circles*). For both tests, relaxation follows an exponential decay with comparable time constants. *Red* and *blue* profiles, respectively, show the exponential fit to the trailing edge of the relaxation signal for Cu-BTC and empty cell. In the inset, the total heat recorded (*filled circles*) and contribution due to spurious heats (*open circles*) for successive dosing steps are given

is linear with incremental pressure (Supplementary information, Fig. S2). This behavior is consistent with the analytical expression: $q_s = -V_0 \, (\alpha_P - \alpha_{ss})T\Delta P$, derived by Mouahid et al. [27], where V_0 is the dead volume of the sample cell measured using helium, α_P and α_{ss} are the isobaric expansion coefficients of hydrogen and stainless steel, respectively. In order to account for the pressure volume work contribution in adsorption experiments, we also performed tests using blank cells with similar pressure and temperature conditions. However, this requires accurately accounting for the volume differences between the empty and MOF-cells and is cumbersome. For most measurements, we directly used the temperature-dependent slope and intercept (Figure S2). Assuming that the spurious heats generated with and without samples are similar, the net heat generated due to adsorption during a step can now be calculated as $q_{net} = q_{total} - q_s$. If Δn_a is the absolute incremental amount of hydrogen adsorbed in each step, the corresponding differential heat of adsorption is:

$$q_d = \frac{q_{net}}{\Delta n_a}. \tag{2}$$

In order to determine Δn_a over the range of adsorbate loading, we measured excess adsorption isotherms simultaneously while the calorimetric runs are being performed (the representative excess adsorption data are shown in the supplementary information, Figure S3). Note that unlike isosteric method, in direct adsorption calorimetry, it is not necessary to perform adsorption isotherms at regularly spaced various temperatures. This is because closely

spaced absolute adsorption can be achieved by combining pressure and temperature conditions. To calculate the corresponding absolute adsorption, we fitted the excess adsorption using the well-known Tóth adsorption model [10, 31]. Tóths model is a modification of Langmuir model that assumes a quasi-Gaussian energy distribution of adsorption sites. This model has already been shown to provide good fits to the hydrogen adsorption isotherms on carbon molecular sieves, zeolite NaX, Cu-BTC, MOF-5, etc. [10]. In the Tóth model, the excess adsorption is related to pressure and temperature of hydrogen as:

$$n_{ex} = n_{max} \frac{bP}{\left(1 + (bP)^n\right)^{1/n}} - \rho v_a, \tag{3}$$

where $b = b_0 \exp(-q_T/RT)$. n is the adsorbent heterogeneity parameter. We used a temperature-dependent n given by $n = n_0 + \alpha T$. b_0, q_T, n_{max}, n_0, α, and v_a are fit parameters obtained using nonlinear regression of excess data using Eq. 3. ρ is the nonideal gas density of hydrogen determined using the equation of state implemented in NIST REFPROP Standard reference database. For two subsequent discrete adsorptions steps i and $i + 1$, $\Delta n_a = n_{ai+1} - n_{ai}$. The corresponding differential heat (q_d) is determined from Eq. 2. Finally, isosteric heat of adsorption is determined using Eq. 4:

$$q_{st} = q_d + zRT, \tag{4}$$

where, z is the compressibility factor determined from the equilibrium pressure and temperature using the real gas EOS and R is the universal gas constant.

4 Adsorption isosteric method

The indirect calculation of isosteric heat based on measuring a series of excess adsorption isotherms over wide temperature ranges is the most prevailing experimental method. The isosteric heat of adsorption for a given surface coverage can be derived to the so-called vańt Hoff form (Eq. 5), which is analogous to the Clausius–Clapeyron equation. A detailed derivation is given elsewhere [32].

$$q_{st} = -R \cdot \left(\frac{\partial \ln(P)}{\partial \frac{1}{T}} \right). \tag{5}$$

From the absolute adsorption isotherms for different temperatures, the logarithm of the pressure values necessary to reach a given absolute adsorption n_a can be plotted versus the reciprocal temperature $1/T$ yielding a linear correlation with a slope proportional to the isosteric heat of adsorption. In this case, the absolute adsorption is calculated from the excess adsorption with approximated excess volume of the adsorbed layer and adsorbed gas density. We assume an

adsorbed layer density close to the liquid hydrogen density ($\rho_l = 0.07$ g ml^{-1}) which remains constant irrespective of the pressure. The absolute adsorption amount is given by:

$$n_{absolute} = n_{excess} \cdot \left(1 + \frac{P \cdot M_{H_2}}{Z \cdot \rho_l \cdot R \cdot T} \right), \tag{6}$$

where z is the compressibility factor and M_{H_2} is de molar mass of the hydrogen. A detail derivation is given in the Supplementary Information.

5 Analytical approach using modified D–A, Unilan, and Tóth adsorption models

Explicit analytical expressions for isosteric heat of adsorption can also be derived by applying such solution thermodynamic formalism as Clausius–Clapeyron relation, to certain empirical adsorption models. In system models, these approaches are preferred over graphical calculation of isotherms as it can generate continuous data without using any interpolation techniques. Here, we consider the analytical expression of isosteric heats by applying the Clausius–Clapeyron relation to three adsorption models: modified DA model [6], Tóth adsorption, and Unilan models [31], summarized in the Table 1. The fit parameters are obtained by nonlinear regression of experimental excess adsorption isotherm measured over wide ranges of pressure and temperature. In addition, we also used an expression for the adsorption isosteric heats based on Tóth adsorption model and Polanyi's potential theory (Tóth's potential function), derived by Whittaker et al. [23]. This method requires only a single adsorption isotherm in contrast to the Clausius–Clapeyron approach. Table 1 lists different analytical expressions used to calculate the isosteric heats.

p^{sat} in the Table 1 is the pseudo-saturation pressure [23]. For isotherms measured at temperatures above the critical temperature of the adsorbate, $p^{sat} = P_c (T/T_c)^2$, where P_c and T_c are the critical pressure and temperature of the gas [17, 23]. n_{max} is the limiting value of absolute adsorption obtained at the limiting pressure P_0, and α_E is the enthalpic contribution of free energy. Note that we use the modified D–A model with a term for heat of vaporization, λ as suggested in recent literature [23]. λ for hydrogen is 0.92 kJ mol^{-1}. The parameters s, x, and a in the Unilan model are, respectively, the difference of the limiting energies ($s = E_{max} - E_{min}$), the ratio of amount adsorbed $\left(x = \frac{n_a}{n_{max}}\right)$ and an integration constant [10].

Figure 3 compares the isosteric heats of hydrogen adsorption on MOF-5, Cu-BTC, MIL-53, MOF-177, and Fe-BTC measured using the adsorption calorimetry, isosteric method, and analytical expressions in the Table 1.

Table 1 Analytical expression of isoteric heats from modified D–A, Tóth, and Unilan by applying Clausius–Clapeyron relation and Tóth's potential function

Model/method	Expression
D–A model/Claus.–Clap.	$Q_{\text{st,DA}} = -\alpha_E \sqrt{\ln\left(\frac{n_a}{n_{\max}}\right)} + \lambda$
Tóth/Claus.–Clap.	$Q_{\text{st,Toth}} = q_T + \frac{\alpha}{n}RT^2\left[\ln\left(\frac{n_a}{n_{\max}}\right)(1 + (bP)^n) - \ln(bP)\right]$
Unilan/Claus.–Clap.	$Q_{\text{st,Unilan}} = E_{\max} - \frac{(1-x)s}{1-\exp\left(\frac{(1-x)s}{RT}\right)} - \frac{xs}{1-\exp\left(\frac{xs}{RT}\right)}$
D–A model/analytical TPF	$Q_{\text{st,DA}} = RT\ln\left(\frac{P^{\text{sat}}}{P} \times \left(\frac{1}{2\left(\frac{RT}{\alpha_E + \beta T}\right)^2 \ln\left(\frac{P_0}{P}\right)} - 1\right)\right) + \lambda + zRT$
Tóth/analytical TPF	$Q_{\text{st,Toth}} = RT\ln\left(\frac{P^{\text{sat}}}{P} \times (bP)^n\right) + \lambda + zRT$
Unilan/analytical TPF	$Q_{\text{st,Unilan}} = RT\ln\left[\frac{P^{\text{sat}}}{P}\left(\frac{n_a}{P}\frac{\left(a + P\exp(E_{\max}/RT)\right)\left(a + P\exp(E_{\min}/RT)\right)}{a\left(\exp\left(E_{\max}/RT\right) - \exp\left(E_{\min}/RT\right)\right)} - 1\right)\right] + \lambda + ZRT$

Fractional coverage is defined as the ratio of the absolute adsorption to the absolute adsorption measured at 77 K and 2 MPa.

For all MOFs, we find a very good agreement between the isosteric heats measured using the calorimetric and isosteric methods throughout the range of loading studied. This is also true for Fe-BTC samples even though the materials used are slightly different (amorphous powder Fe-BTC is used for calorimetric measurements, while xerogel Fe-BTC is used in adsorption isosteric method). In the low coverage when $n_a < 5$ mol kg^{-1} (fractional coverage < 2 %), q_{st} of Cu-BTC is 5.9 kJ mol^{-1} at 2.9 mol kg^{-1} and is the highest among the MOFs, and decreases in the order MIL-53 > MOF-5 > Fe-BTC > MOF-177. For extended network materials like MOFs, the evolution of adsorption isosteric heat as a function of adsorbate loading is decided by their two unique pore structures: pore dimension and exposed unsaturated metal centers [13]. Higher surface curvature of small pores provides stronger interaction with adsorbates; this causes smaller pores to be preferentially occupied at lower loading. Also, metal centers, such as binuclear Cu$^+$ in thermally activated Cu-BTC, acts as Lewis acid sites that offer strong interaction with the adsorbates. Since such sites are few, we expect them to be filled at the onset of adsorption. Cu-BTC structure consists of two type of cages; larger cages with diameters 9 Å and tetrahedral side pockets of roughly 6 Å diameter [13, 33]. MIL-53 has only one type of pores having a diameter of 8.5 Å [34]. Pores in the MOF-5 can have diameter 12 or 15 Å depending on the orientation of the benzene ring [13, 33]. Likewise, MOF-177's pore diameters are 11 and 19 Å depending on the orientation of the benzene rings [33, 35]. The higher isosteric heat of Cu-BTC at the onset of adsorption can be attributed to its smallest pores and availability of unsaturated Cu$^+$ sites. As adsorption increases, larger pores of 11.8 Å becomes accessible; this causes the isosteric heat of Cu-BTC to fall below that of MIL-53. It eventually crosses over the isosteric heats of MOF-5 and MOF-177. This crossover occurs due to lower adsorption capacity of MIL-53 and Cu-BTC as compared with MOF-5 and MOF-177 (observed in low-pressure nitrogen adsorption, see supplementary information). The order of isosteric heats in Cu-BTC, MIL-53, and MOF-5 is coherent with the hydrogen's interaction strength revealed from thermal desorption spectroscopy (TDS) measurements. Temperatures at which hydrogen desorption rates form maxima or shoulders in the TDS spectrum ($T_{\max}$) represent direct measures of the strength of hydrogen's interaction with the MOF's adsorption sites; the peaks for MOFs were observed at 53 (Cu-BTC), 45 (MIL-53) and 40 K (MOF-5) [36, 37].

At the vicinity of saturation, the contribution of differential heat of adsorption (q_d) to adsorption vanishes and isosteric heat will be constant equal to the heat of vaporization of hydrogen (0.9 kJ mol^{-1}). Throughout the coverage examined in this work, the isosteric heat is larger than the heat of vaporization of hydrogen. This means molecules within the micropores always feel the potential field and does not show any saturation unlike what happens the adsorption occurs on the external surface of the material.

6 Conclusions

In this work, we compared the isosteric heats of hydrogen adsorption on microporous materials measured directly using adsorption calorimetry with those obtained using indirect adsorption isosteric method and using modified D–A, Tóth, and Unilan adsorption analytical models so as to establish the reliability and limitations of methods and assumptions. For the first approach, the absolute adsorption was derived using the analytical Tóth adsorption model, and the real gas density of hydrogen was calculated from
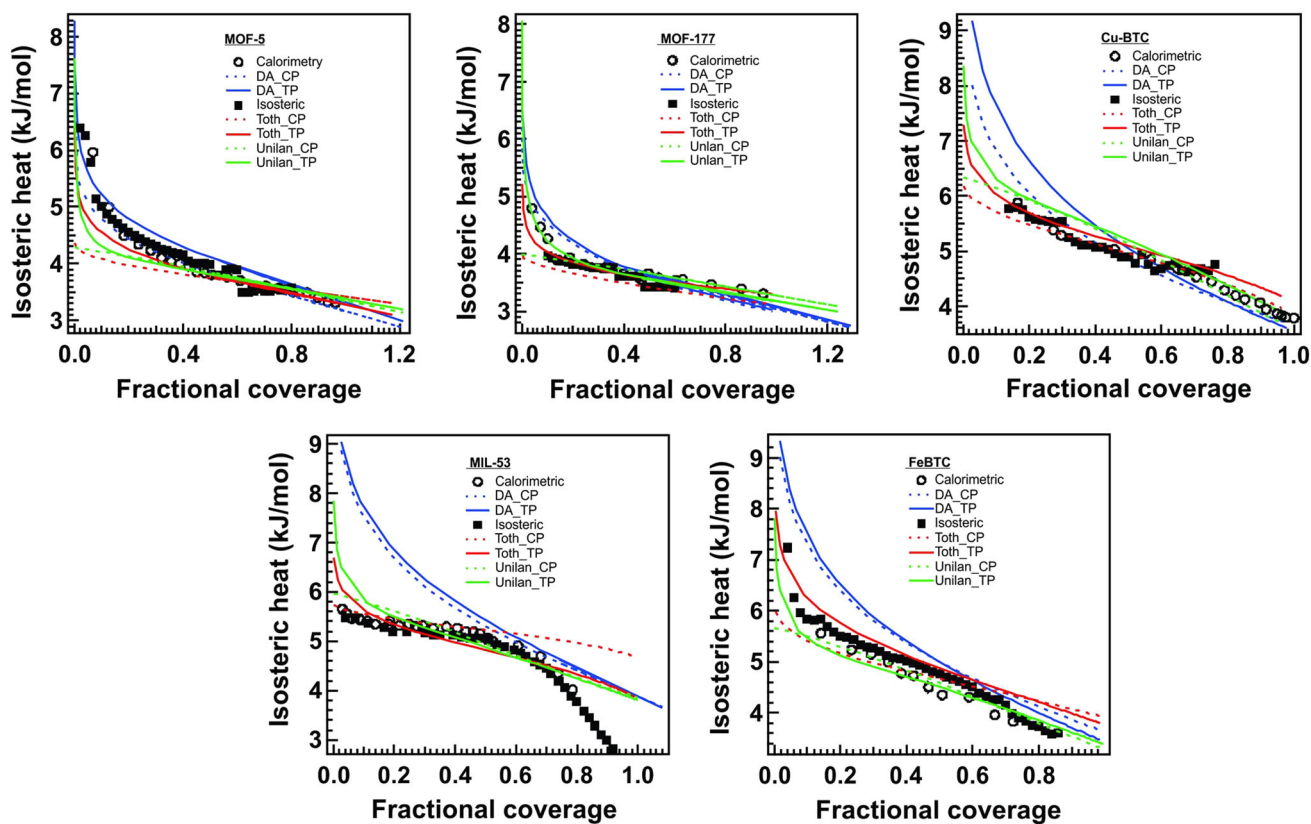
Fig. 3 Comparison of the adsorption isosteric heats of MOFs measured using coupled adsorption calorimetry with those obtained using sorption isosteric technique

real gas EOS implemented in the NIST REFPROP Standard reference database. For the indirect adsorption isosteric method, the absolute adsorption was derived by assuming a constant liquid density for the adsorbed hydrogen and a gas density corresponding to ideal gas EOS with a compressibility factor correction.

For all MOFs, we find a very good agreement between the isosteric heats measured using the adsorption calorimetric and adsorption isosteric methods throughout the range of loading studied. Therefore, we can conclude that the use of the simpler technique, i.e., adsorption isosteric method together with simple assumptions lead to reliable results for isosteric heats. Isosteric heats predicted using the analytical models on the other hand deviate from both experiments depending on the MOF studied and the range of loading. Under low-loadings of less than 5 mol kg^{-1}, the isosteric heat of hydrogen adsorption decreases in the order Cu-BTC > MIL-53 > MOF-5 > Fe-BTC > MOF-177. The order of isosteric heats is coherent with the strength of hydrogen interaction revealed from previous thermal desorption spectroscopy measurements.

References

1. J.K.N. Newhouse, in *Proceedings of Annual Merit Review Meetings of US DOE* (2014), http://www.hydrogen.energy.gov/pdfs/review14/st047_newhouse_2014_o.pdf
2. Y.-S. Bae, R.Q. Snurr, Microporous Mesoporous Mater. **132**, 300 (2010)
3. B. Hardy, C. Corgnale, R. Chahine, M.-A. Richard, S. Garrison, D. Tamburello, D. Cossement, D. Anton, Int. J. Hydrogen Energy **37**, 5691 (2012)
4. S. Ubaid, R. Zacharia, J. Xiao, R. Chahine, P. Bénard, P. Tessier, Int. J. Hydrogen Energy **40**, 9314 (2015)
5. J. Bear, Y. Bachmat, *Introduction to Modeling of Transport Phenomena in Porous Media* (Kluwer Academic Publishers, The Netherlands, 1991)
6. M.-A. Richard, D. Cossement, P.-A. Chandonia, R. Chahine, D. Mori, K. Hirose, AIChE J. **55**, 2985 (2009)
7. E. Dundar, R. Zacharia, R. Chahine, P. Benard, Fluid Phase Equilibr **363**, 74 (2014)
8. J. Xiao, L. Tong, C. Deng, P. Bénard, R. Chahine, Int. J. Hydrogen Energy **35**, 8106 (2010)
9. L.J. Murray, M. Dinca, J.R. Long, Chem. Soc. Rev. **38**, 1294 (2009)

10. J. Purewal, D. Liu, A. Sudik, M. Veenstra, J. Yang, S. Maurer, U. Müller, D.J. Siegel, J. Phys. Chem. C **116**, 20199 (2012)
11. A. Dailly, J.J. Vajo, C.C. Ahn, J. Phys. Chem. B **2006**, 110 (1099)
12. B. Panella, M. Hirscher, H. Pütter, U. Müller, Adv. Funct. Mater. **16**, 520 (2006)
13. B. Schmitz, U. Müller, N. Trukhan, M. Schubert, G. Férey, M. Hirscher, ChemPhysChem **9**, 2181 (2008)
14. W. Zhou, H. Wu, M.R. Hartman, T. Yildirim, J. Phys. Chem. C **111**, 16131 (2007)
15. S.S. Kaye, A. Dailly, O.M. Yaghi, J.R. Long, J. Am. Chem. Soc. **129**, 14176 (2007)
16. M. Schlichtenmayer, B. Streppel, M. Hirscher, Int. J. Hydrogen Energy **36**, 586 (2011)
17. S. Ozawa, S. Kusumi, Y. Ogino, J. Colloid Interface Sci. **56**, 83 (1976)
18. A. Züttel, P. Sudan, P. Mauron, P. Wenger, Appl. Phys. A **78**, 941 (2004)
19. N.P. Stadie, Dissertation (Ph.D.), California Institute of Technology (2013)
20. J. Purewal, Dissertation (Ph.D.), California Institute of Technology (2010)
21. W. Zimmermann, J.U. Keller, Thermochim. Acta **405**, 31 (2003)
22. E.W. Lemmon, M.L. Huber, M.O. McLinden, in *NIST Standard Reference Database 23: Reference Fluid Thermodynamic and Transport Properties-REFPROP, Version 9.1, National Institute of Standards and Technology, Standard Reference Data Program, Gaithersburg, 2013* (National Institute of Standards and Technology, 2013)
23. P.B. Whittaker, X. Wang, K. Regenauer-Lieb, H.T. Chua, Phys. Chem. Chem. Phys. **15**, 473 (2013)
24. R. Zacharia, D. Cossement, L. Lafi, R. Chahine, J. Mater. Chem. **20**, 2145 (2010)
25. E. Poirier, R. Chahine, P. Bénard, L. Lafi, G. Dorval-Douville, P.A. Chandonia, Langmuir **22**, 8784 (2006)
26. G. Dorval-Douville, Master Thesis, Université du Québec a trois rivieres (2006)
27. A. Mouahid, D. Bessieres, F. Plantier, G. Pijaudier-Cabot, J. Therm. Anal. Calorim. **2012**, 109 (1077)
28. L.E. Vilchiz-Bravo, A. Pacheco-Vega, B.E. Handy, Meas. Sci. Technol. **21**, 115103 (2010)
29. L.E. Vilchiz, A. Pacheco-Vega, B.E. Handy, Thermochim. Acta **439**, 110 (2005)
30. J.A. Dunne, M. Rao, S. Sircar, R.J. Gorte, A.L. Myers, Langmuir **12**, 5896 (1996)
31. K.Y. Foo, B.H. Hameed, Chem. Eng. J. **156**, 2 (2010)
32. F.o. Rouquerol, J. Rouquerol, K.S.W. Sing, *Adsorption by Powders and Porous Solids: Principles, Methodology, and Applications* (Academic Press, San Diego, 1999)
33. M. Schlichtenmayer, M. Hirscher, J. Mater. Chem. **22**, 10134 (2012)
34. S. Bourrelly, P.L. Llewellyn, C. Serre, F. Millange, T. Loiseau, G. Férey, J. Am. Chem. Soc. **127**, 13519 (2005)
35. S. Maurice, Ph.D. Thesis, Max-Planck-Institut für Intelligente Systeme, Stuttgart (2012)
36. B. Panella, K. Hones, U. Muller, N. Trukhan, M. Schubert, H. Putter, M. Hirscher, Angew. Chem. Int. Edit. **47**, 2138 (2008)
37. I. Krkljus, M. Hirscher, Microporous Mesoporous Mater. **142**, 725 (2011)